SECURITY CLASSIFICATION OF THIS PAGE

REPORT DOCUMENTATION PAGE

AD-A244 936

1a. REPORT SECURITY CLASSIFICATION	**1b. RESTRICTIVE MARKINGS**
2a. SECURITY CLASSIFICATION AUTHORITY	**3. DISTRIBUTION / AVAILABILITY OF REPORT**
2b. DECLASSIFICATION / DOWNGRADING SCHEDULE	Approved for public release; distribution unlimited.
4. PERFORMING ORGANIZATION REPORT NUMBER(S) --	**5. MONITORING ORGANIZATION REPORT NUMBER(S)** *MIPR ARO 114-91*

6a. NAME OF PERFORMING ORGANIZATION Naval Postgraduate School Navy-NASA Joint Instt. of Aero.	6b. OFFICE SYMBOL *(If applicable)* Code AA/CH	7a. NAME OF MONITORING ORGANIZATION U. S. Army Research Office
6c. ADDRESS (City, State, and ZIP Code) Dept. of Aero. & Astro. Monterey, CA 93943		7b. ADDRESS (City, State, and ZIP Code) P. O. Box 12211 Research Triangle Park, NC 27709-2211

8a. NAME OF FUNDING / SPONSORING ORGANIZATION U. S. Army Research Office	8b. OFFICE SYMBOL *(If applicable)*	9. PROCUREMENT INSTRUMENT IDENTIFICATION NUMBER *ARO 27894.9-EG*

8c. ADDRESS (City, State, and ZIP Code) P. O. Box 12211 Research Triangle Park, NC 27709-2211	10. SOURCE OF FUNDING NUMBERS			
	PROGRAM ELEMENT NO.	PROJECT NO.	TASK NO.	WORK UNIT ACCESSION NO.

11. TITLE (Include Security Classification)
A Real Time Interferometry System for Unsteady Flow Measurements (unclassified).

12. PERSONAL AUTHOR(S)
N. J. Brock, M. S. Chandrasekhara and L. W. Carr

13a. TYPE OF REPORT Reprint	13b. TIME COVERED FROM ___ TO ___	14. DATE OF REPORT (Year, Month, Day) Oct. 25-28.1991	15. PAGE COUNT 8

16. SUPPLEMENTARY NOTATION The view, opinions and/or findings contained in this report are those of the author(s) and should not be construed as an official Department of the Army position, policy, or decision, unless so designated by other documentation.

17.	COSATI CODES		18. SUBJECT TERMS (Continue on reverse if necessary and identify by block number)
FIELD	GROUP	SUB-GROUP	Interferometry, Real-Time techniques, Unsteady Flows, Dynamic Stall

19. ABSTRACT (Continue on reverse if necessary and identify by block number)
A simple real-time interferometer system was developed for use in dynamic stall and other unsteady flow research at compressible flow speeds. A conventioned schlieren system was modified to operate as a point diffraction interferometer. The implementation of this interferometer is discussed and results of trails with different point diffractors are presented in this paper. The performance of the interferometer under various flow conditions was investigated. Results are presented which show the effects of the interferometer parameters such as pinhole size and pinhole-plate optical density on the performance of the system.

92-00524

20. DISTRIBUTION / AVAILABILITY OF ABSTRACT ☒ UNCLASSIFIED/UNLIMITED ☐ SAME AS RPT. ☐ DTIC USERS	21. ABSTRACT SECURITY CLASSIFICATION Unclassified
22a. NAME OF RESPONSIBLE INDIVIDUAL	22b. TELEPHONE (Include Area Code) 22c. OFFICE SYMBOL

DD FORM 1473, 84 MAR   83 APR edition may be used until exhausted.   SECURITY CLASSIFICATION OF THIS PAGE
All other editions are obsolete.   UNCLASSIFIED

ICIASF '91
RECORD

International Congress on Instrumentation in
Aerospace Simulation Facilities

Rockville, MD
October 25 - 28, 1991

A Real Time Interferometry System for Unsteady Flow Measurements

N.J. Brock
Scientist
Aerometrics, Inc.,
550 Del Rey Avenue, Unit A, Sunnyvale, CA 94086

M.S. Chandrasekhara
Adjunct Research Professor and Assistant Director
Navy-NASA Joint Institute of Aeronautics
Fluid Mechanics Laboratory, NASA Ames Research Center
Department of Aeronautic. nd Astronautics
Naval Postgraduate School, Monterey, CA 93943

L.W. Carr
Group Leader, Unsteady Viscous Flows
Aeroflightdynamics Directorate, U.S. Army AVSCOM, and
Fluid Mechanics Laboratory, NASA Ames Research Center
Moffett Field, CA 94035

ABSTRACT

A simple real-time interferometer system was developed for use in dynamic stall and other unsteady flow research at compressible flow speeds. A conventional schlieren system was modified to operate as a p int diffraction interferometer. The implementation of this interferometer is discussed and results of trials with different point diffractors are presented in this paper. The performance of the interferometer under various flow conditions was investigated. Results are presented which show the effects of the interferometer parameters such as pinhole size and pinhole-plate optical density on the performance of the system.

1. INTRODUCTION

Unsteady flow measurements, especially at high subsonic speeds, pose significant challenges to experimental fluid dynamicists. The problem becomes even more complex when flow separation is encountered. Much of the measurement difficulty stems from the character of the flow under investigation. The flow is rapidly changing in a high speed environment, thus invalidating many conventional flow visualization techniques. There is a critical need for details of the flow away from the surface, thus limiting the value of instantaneous pressure transducers. The flow contains significant regions of separation, thus invalidating the use of hot wire anemometry. The fluid experiences very strong pressure gradients ($\frac{dC_p}{dx} \sim O(10^3)$), and velocity gradients(e.g. shocks), thus severely limiting the use of particle-based measurement techniques such as LDV or laser speckle velocimetry. Also, the repetitive sampling needed to obtain statistically invariant data in these flows requires operating the

drive mechanism that produced the unsteady flow for times and loads that can exceed the fatigue life of the system. These stringent measurement requirements leave only those techniques which exploit the instantaneously changing flow properties (e.g. density) for use in diagnosis of the flow properties. A stroboscopic schlieren technique has already been implemented for study of this flow[1], but it gives only qualitative information about the flow field. The quantitative technique of interferometry becomes the logical choice in these flow situations. It offers many advantages since the entire flow field can be imaged, and the visualization does not depend on any particle tracker. However, conventional interferometry methods such as Mach-Zehnder interferometry require expensive and very high quality optical components, set up in a vibration-free environment, in order to work satisfactorily - conditions made more difficult in a high speed, dynamic flow facility. The more forgiving method of holographic interferometry suffers from the drawback that significant post-processing must be performed for an interferogram to be obtained.

The present paper describes a point diffraction interferometer(PDI) now successfully being used in dynamic stall research under compressible flow conditions. (For details of the research findings, see ref. 2 and 3). The PDI is a simple real time interferometer that produces interferograms that are equivalent to interferograms produced by Mach-Zehnder and holographic interferometers[4]. However, it has an advantage over these interferometers because it is a common path interferometer which makes it much less sensitive to vibration. Furthermore, since an existing schlieren system can be easily modified into a PDI system, it is inexpensive to implement. PDI was originally applied to optical testing[5,6], and has only recently been applied to fluid flow research[7]. This paper explores the issues that arose during the implementation of the PDI technique in research undertaken to determine the influence of compressibility on dynamic stall.

2. DESCRIPTION OF EXPERIMENT

2.1. Experimental Facility

The studies were carried out in the Compressible Dynamic Stall Facility(CDSF), at the Fluid Mechanics Laboratory of the NASA Ames Research Center. The CDSF test section size is 25cm X 35cm, and the tunnel Mach number ranges from M = 0.1 - 0.5. A schematic of the CDSF is shown in Fig. 1. The CDSF is equipped with a drive mechanism that simultaneously oscillates two windows in simple harmonic motion. The airfoil is supported between the windows and this results in a sinusoidal variation of its angle of attack. Depending upon the research problem under investigation, the oscillating drive can be replaced by a hydraulic drive that produces a rapid ramp type pitch-up motion. Both drives are instrumented with incremental encoders that provide the airfoil instantaneous angle of attack information digitally which is used in performing stroboscopic measurements.

2.2. Optical System

The optical system used is shown in Fig. 2. A conventional two-mirror schlieren imaging system was modified by replacing the spark light source with a Nd-YAG laser and the knife edge with a pinhole-plate to create the PDI system discussed in this paper. The laser light was expanded to fill a portion of the first schlieren mirror, where it was reflected through the test section and refocused on to the pinhole plate by the second schlieren mirror. A camera placed at the image plane of the mid-span of the flow recorded the interference pattern created. The astigmatism inherent to the original 'Z' configuration was reduced by using an on-axis alignment, wherein only a portion of each schlieren mirror aperture was used so that the beam-expanding lens and the pinhole could be located on-axis at the foci of the respective mirrors. This alignment was made possible by the large diameter (450mm) schlieren mirrors relative to the small diameter (150mm) of the test section windows.

3. THE PDI TECHNIQUE

3.1 Description of the PDI Technique

In a PDI system, light from a point source is collimated and is then directed through a flow field after which it is focused onto a pinhole in a partially-absorbing plate(see Figure 3). The light that passes around the pinhole is attenuated, but still retains the phase information induced by the flow field. Light which passes through the pinhole is diffracted into a spherical reference wave, (provided the pinhole is sufficiently small) and makes the pinhole a local point source. Light diffracting from this local point source interferes with the undiffracted light passing around the pinhole. The real-time interference fringes produced by this method provide instantaneous contours of constant optical path difference caused by density variations in the flow field under study.

The quality of the interferograms that are obtained by PDI is dependent upon several parameters: for example, the transmittance of the pinhole plate, τ_b; the diameter of the pinhole, d; the amount of light passing through the pinhole and around it; and the optical path difference introduced by the flow density changes. Therefore, a review of the theory behind point diffraction interferometry is of some use in studying these parameters. The complex amplitude distribution of light at the image plane can be derived using Fourier theory[8]. The derivation is similar to that shown by Koliopoulos et al[5] in the derivation of a point diffraction interferometer for optical testing, the main difference being the location of the object being studied.

The complex amplitude distribution of the light leaving a circular window of the wind tunnel test section can be written as

$$u_0(x,y) = Cyl(\frac{r}{D})e^{jkW(x,y)} \qquad (1)$$

assuming a two dimensional flow, $r = \sqrt{x^2 + y^2}$ is any point in the plane of the window, D is the window diameter, $k = \frac{2\pi}{\lambda}$ is the wave number(with λ as laser light wave length) and W(x,y) represents the optical path differences due to density variations of the flow. The cylinder function (defined in Ref. 8) as a function of value 1 for $0 \leq r \leq D$, and 0 for $r > D$,describes the transmittance of light through a circular aperture. The amplitude transmittance of the pinhole plate can be shown to be

$$t(x,y) = \tau_b + (1 - \tau_b)Cyl(\frac{r}{d}) \qquad (2)$$

where d is the diameter of the totally transparent pinhole, and τ_b, which is related to the optical density, is the transmittance of the substrate surrounding the pinhole. The complex amplitude distribution of the light $u_i(x,y)$ at the image plane is the convolution of the complex amplitude distribution of the light leaving the test section window (Eqn 1) with the Fourier transform of the pinhole plate amplitude transmittance function (Eqn 2). After some operations and simplifications, and the neglecting of optic focal length terms which affect image size only, and of an unimportant phase factor which does not affect the resultant interferograms, the complex amplitude distribution becomes

$$u_i(x,y) = \tau_b\, Cyl\left(\frac{r}{D}\right)e^{jkW(x,y)} \; +$$

$$\left\{ \left[Cyl\left(\frac{r}{D}\right)e^{jkW(x,y)} \right] \; * \right.$$

$$\left. \left[(1 - \tau_b)\frac{\pi}{4}\left(\frac{d}{\lambda f_2}\right)^2 \right] Somb\left(\frac{rd}{\lambda f_2}\right) \right\} \qquad (3)$$

where * denotes convolution and f_2 is the focal length of mirror 2. The Sombrero function used above describes the response of an imaging system with a circular limiting aperture to a point source and is defined as[8]

$$Somb\left(\frac{rd}{\lambda f_2}\right) = \frac{2J_1\left(\frac{\pi r d}{\lambda f_2}\right)}{\left(\frac{\pi r d}{\lambda f_2}\right)}$$

where J_1 is the Bessel function of the first order and first kind.

As explained earlier, the two terms described in eq. (3) interfere at the image plane. The first term, which is the object wave, is the original aberrated wavefront reduced in amplitude by τ_b, and represents the light passing around the pinhole. The second term is the reference wavefront resulting from the convolution of the aberrated wavefront from the test section with the Fourier transform of the pinhole transmittance.

If W(x,y) were known, the dependence of reference and object wave amplitude on optical plate transmittance and pinhole diameter could be determined from this equation. However, this task is not trivial even if W(x,y) could be approximated. Therefore, the dependence of the resultant interferograms on pinhole size and optical density of the pinhole plate were determined experimentally for the present application.

3.2. Implementation

3.2.1. Pinhole Plate

The pinhole plate used in this experiment was made from a photographic plate (Agfa 8E75HD). The plate was processed in a weak developer (2-3% solution of triethanolamine), dried and then exposed uniformly to light in order to darken it. No other processing was required. Darkened plates with optical densities near 1 were used for the flow conditions of this test; this absorption level was necessary to attenuate the object wave to a level equal in intensity to that of the reference wave, in order to maximize fringe contrast.

3.2.2. Creation of Pinholes

Diffracting spots and pinholes were made by placing the pinhole plate precisely at the focus of the second schlieren mirror, and repeatedly pulsing the laser with no flow in the test section. The laser energy was slowly increased, while observing the effect of the laser pulses on the pinhole plate as seen on a screen placed at the image plane. When the laser energy was sufficiently high to char a spot(as is done in dark central ground interferometry(DCGI)), the image turned black. When the spot was burned with sufficient number of pulses and energy the image turned white, indicating that a pinhole had formed. The size of the spot or pinhole could be varied by carefully controlling the laser energy. Once the spot or pinhole was made, it was left in place and the laser energy was decreased to a level that adequately exposed the camera film without burning the pinhole further.

4. RESULTS AND DISCUSSION

4.1. PDI vs. DCGI

Initial interferometer development efforts for the CDSF were focused on holographic interferometry. However, since the ultimate goal of this effort was to produce real-time interferograms in high speed, strongly unsteady flows, various types of real time interferometry were investigated. The first technique to be studied was dark-central-ground interferometry(DCGI), which is based on the same principles as PDI, but uses a small opaque spot to generate the reference wave. For small spots or pinholes, it has been shown[4,9] that DCGI actually produces fringes with greater contrast and intensity than PDI. However, the PDI pinhole is able to withstand higher energy laser pulses, since the peak energy portion of the beam is passed through the pinhole instead of absorbed by the pinhole plate. This is an important factor in the present application and in future high speed applications where an extremely short light pulse is necessary to freeze the fast moving fringes that occur in the flow which were induced by the rapidly pitching airfoil; at the same time, the laser pulse must have sufficient energy to expose the film at the image plane. During the work with DCGI, it was found that laser pulses containing sufficient energy to expose film at the image plane destroyed the spots by actually burning through the emulsion on the pinhole plate. Reducing the size of the interferogram on the film by using imaging lenses concentrated the light for a brighter exposure, but at the cost of reduced image resolution.

In recent efforts, photographically fixed plates with reduced absorption enabled the creation of spots that could withstand the high laser energy levels, and full size interferograms were obtained. However, the fringe contrast was much lower than what had already been achieved with PDI[2,3]. Hence, further development of DCGI for the facility was discontinued.

4.2. Effect of Pinhole Size

The size range of pinholes that were used in the system was determined by the magnitude of the density gradients and the size of the system blur circle at the focus of mirror 2 (the blur circle is defined as the size of the image of a point source formed by a lens at its focus). For most applications, good quality, high contrast fringes are obtained with a pinhole approximately the size of the system Airy disk[6]. The Airy disk diameter is equal to 2.44 λ f # (where f # is the "f-stop" of the mirror) and is defined as the area of the central peak of the diffraction pattern formed at the focus of a uniformly illuminated, unaberreted optic. This ideal, diffraction limited focal point was calculated to be 25μm for mirror 2. The actual size of the focus of the miror was larger than the Airy disk due to aberrations, however, the Airy disk size served as a good rule of thumb. The size of the pinhole could be varied from this ideal size to enhance certain characteristics of the interferometer. Small pinholes ($\leq$ 25μm in the present application) made the interferometer more sensitive to low frequency fringes caused by mild density variations. Since the pinhole

was a high pass filter, increasing its size increased the amount of low frequency information that was filtered. However, high frequency information resulting from strong density gradients was essentially unaffected by this filter. Therefore, larger pinholes could be used when imaging high frequency fringes such as those that occur near the airfoil leading edge. The flow region of greatest interest in the present study was the upper surface of the airfoil near the leading edge. Since the fringes produced by the strong gradients that existed in this region were of high frequency, the fringes were unaffected by the low frequency filtering of the large pinholes. (See Fig. 4-7).

All the PDI interferograms obtained during this study were recorded on Polaroid Type 57 (ASA 3000) film without damage to the pinhole. However, when an attempt was made to expand the recorded image size in order to increase the detail of the region near the leading edge, the problem of pinhole enlargement was encountered. This could be directly attributed to the fact that the higher image magnification reduced the amount of light at the image plane, and the increased laser energy needed to offset this for proper film exposure caused the pinhole to burn and become enlarged. To quantify the effect of this enlargement of the pinhole size, interferograms of the same flow at the same conditions were obtained with a small ($25\mu m$) pinhole and a large ($80\mu m$) pinhole. The interferograms of Figure 4 were made with the small pinhole. Fig.4a shows the flow field at an angle of attack, $\alpha = 0^0$ and a Mach number, $M = 0.4$. The good symmetry of the flow over the airfoil can easily be seen, including at the trailing edge. The fringes are complete and show good contrast over the whole flow field. Fig. 4b shows the density field at $\alpha = 8^0$, $M = 0.4$. Once again, the fringes appear good throughout the flow field. Even the airfoil boundary layer can be clearly seen. The interferograms presented in Fig. 5a and 5b record the same flow at the same conditions as in Fig. 4, but were made with the large pinhole. It can be seen that the fringes away from the airfoil are distorted. In addition, many of the fringes away from the airfoil fade and eventually disappear. However, the fringes near the airfoil leading edge are unchanged, are of high contrast, and are in good agreement with the corresponding images in Fig. 4.

For the interferograms in Fig. 6a and 6b, the imaging optics were changed to provide larger and more detailed images on film for the same flow conditions investigated in Fig. 4 and 5. The images in Fig. 6 were recorded using the large pinhole. Only the large pinhole passed sufficient light for a good photograph to be obtained. Hence, the two interferograms shown in Fig. 4a and 4b were photographically enlarged and are shown in Fig. 7a and 7b for comparison with Fig. 6a and 6b. The same details of the densely packed fringes can be seen in the leading edge region in both sets of photographs. The fringes in this region of strong density gradients have high contrast and are continuous. The two sets of pictures agree very well, except that the resolution in Fig. 7 is not very good in comparison to Fig. 6; this demonstrates the limitations of photographic enlargement for study of the leading edge region.

Thus, for fluid flow applications with strong den-

sity gradients such as those encountered in the present set of experiments, sensitivity to low frequency fringes (such as those away from the airfoil), is not always necessary. Therefore, interferograms made with large pinholes, which have been shown to provide accurate fringes in dense gradient regions, are sufficient. Furthermore, the increase in light at the image plane made available by use of the large pinholes allows enlarged images to be captured on film, thus providing for higher resolution.

4.3. Effects of Flow Conditions

The flow conditions encountered in the CDSF cover a range of angles of attack from 0 to 60 degrees and a Mach number range from 0.1 - 0.5. Thus, large density variations were present in the flow. The effect of the density gradients in the flow is to spread out the light which was focused on the pinhole plate. The strength of the gradients to be imaged determined the amount of spreading. At low Mach numbers and low angles of attack, the gradients were weak; however, they were strong at high Mach numbers, even at low angles of attack. Obviously, the degree of light spreading was dependent upon the flow conditions. In flows with strong density gradients, refracted light could be seen up to 30mm away from the optical axis at the focal plane. Although this light was very faint, obscuring it caused image distortions. Hence, it was important that all the light passing through the test section fell on the pinhole plate.

In an effort to study the effects of flow conditions on light spreading, a CCD camera was placed at the focus of mirror number 2 and the focused light was recorded and digitized for three flow conditions: $\alpha = 0^0$, no flow; $\alpha = 0^0$, $M = 0.4$; and $\alpha = 8^0$, $M = 0.4$. Light intensity variations along a horizontal row of pixels passing through the central peak of the image at the focus were then obtained and are plotted in Fig. 8 for these conditions. The CCD was allowed to saturate in the central region in order to enhance the details of the outer lower intensity regions. As can be seen from Fig. 8, the spread of the light is about 20 pixels for the no flow case. With the flow on, at $\alpha = 0^0$, it is about 25 pixels, but at $\alpha = 8^0$, it is 50 pixels. It should be noted that in this figure, 100 pixels correspond to 1 mm, and hence, a pinhole of $80\mu m$ is about 10 pixels wide.

For maximum fringe contrast, as mentioned earlier, the intensity of the light diffracted from the pinhole should equal the intensity of the object wave passing around the pinhole. This balance was sometimes altered when the spread of the light was changed due to the changing flow conditions. However, if the pinhole size and the optical density of the plate were properly selected, high contrast interferograms could be obtained for a broad range of flow conditions[3].

4.4. Effects of Pinhole Plate Material

Both PDI and DCGI are limited by the amount of energy that the pinhole plate can absorb without destroying the point diffractor. In addition to the AGFA photographic plate used in the present test, both blue and green line filters were used as pinhole

plates in previous tests and were found to work well[2]. However, pinholes made from line filters could not withstand the energy that the AGFA plates could. Since the AGFA plate emulsion is thicker than that of the line filter, it is possible that the former could dissipate the energy faster. More research is needed to find better pinhole-plate materials, especially for the very high laser-pulse repetition rates needed for the high-speed filming of dynamic stall development that are planned in the future.

5. CONCLUSIONS

Point diffraction interferometry has been shown to be a very valuable tool for quantitative visualization of dynamic stall flow fields in compressible flow. It has been shown that when large pinholes were used for PDI, the interferometer was insensitive to small density changes in regions of low density gradients. However, the sensitivity in regions of large density gradients was not significantly affected. The increase in image brightness due to the large pinholes was found to be necessary for recording the enlarged details of selected regions of the flow. Interferograms made with large pinholes compared well with those obtained with small pinholes in the region of the leading edge. Thus, when using PDI for imaging strong density gradients, pinholes larger than the Airy disk of the optic focussing on to the pinhole plate can be used without significant loss of quantitative flow field information and fringe quality.

ACKNOWLEDGEMENTS

6. REFERENCES

1. M.S. Chandrasekhara and L.W. Carr, "Flow Visualization Studies of the Mach Number Effects on the Dynamic Stall of an Oscillating Airfoil", *Jl. of Aircraft*, Vol. 27, No. 6, pp. 516-522, June 1990.

2. L.W. Carr, M.S. Chandrasekhara, S. Ahmed, and N.J. Brock, "A Study of Dynamic Stall Using Real Time Interferometry", AIAA Paper No. 91-0007, Presented at the AIAA 27th Aerospace Sciences Meeting, Reno, NV, Jan. 7-11, 1991

3. L.W. Carr, M.S. Chandrasekhara and N.J. Brock, "A Quantitative Study of Unsteady Compressible Flow Over an Oscillating Airfoil", AIAA Paper No. 91-1683, Presented at the AIAA 22nd Fluid Dynamics, Plasma Dynamics and Lasers Conference, Honolulu, HI, June 24-27, 1991.

4. R.C. Anderson, and J.E. Milton, "A Large Aperture Inexpensive Interferometer for Routine Flow Measurements", ICIASF'89 RECORD, IEEE Publication 89CH2762-3, pp. 394-399.

5. C. Koliopoulos, O. Kwon, R. Shagam, and J.C. Wyant, "Infrared Point Diffraction Interferometer", *Optics Letters*, Vol. 3., No. 3, Sept. 1978.

6. R.N. Smartt and W.H. Steel, "Theory and Application of Point Diffraction Interferometers", *Japan Jl. of App. Phys.*, Vol. 14, 1975, Suppl. 14-1.

7. W.D. Bachalo, and M.J. Houser, "Evaluation and Application of a New Technique for Compressible Flow Research", NASA CR-177467, Oct. 1988.

8. J.D. Gaskill, "Linear Systems, Fourier Transforms and Optics", John Wiley and Sons, New York 1978.

9. R.C. Anderson, and J.E. Milton, "Conversion of Schlieren Systems to High Speed Interferometers", *citation not available.*
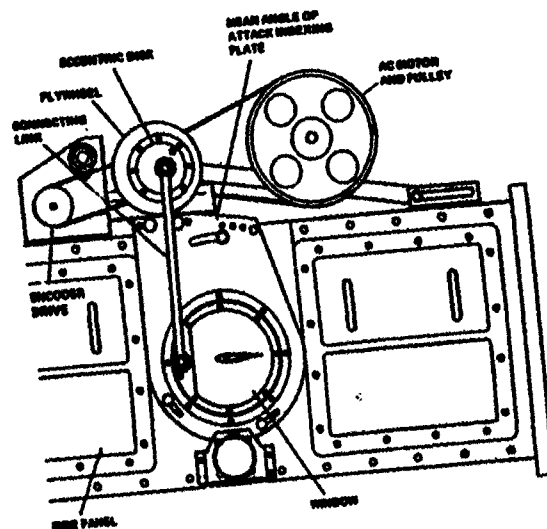
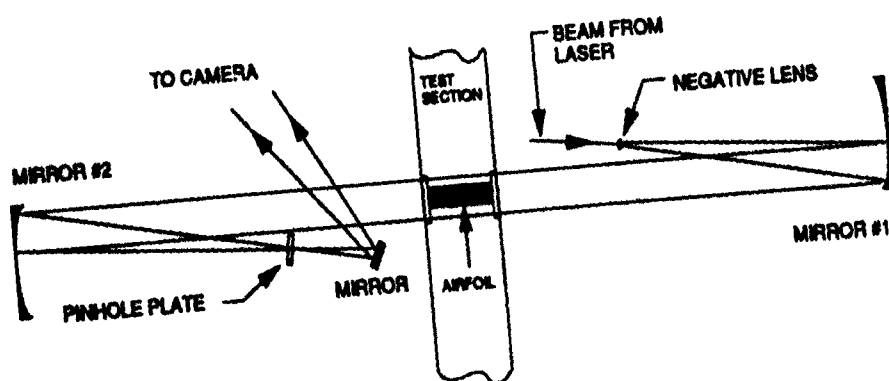Fig. 1. Schematic of CDSF Test Section.

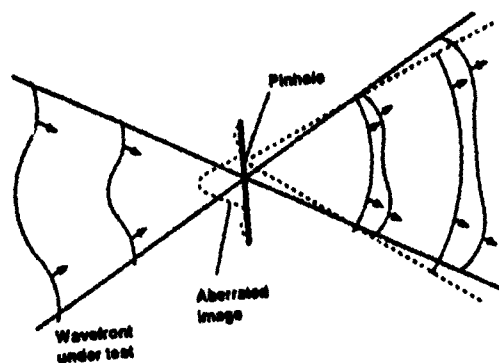Fig. 2. Schematic of the Point Diffraction Interferometer.

Fig. 3. Principle of Point Diffraction Interferometry.

(a)

(a)

(b)

(b)

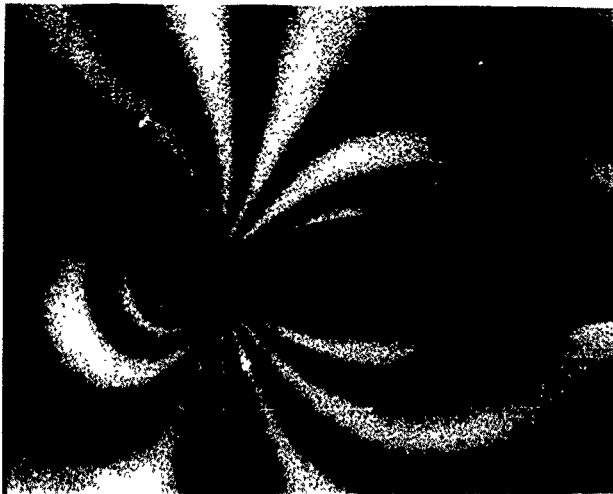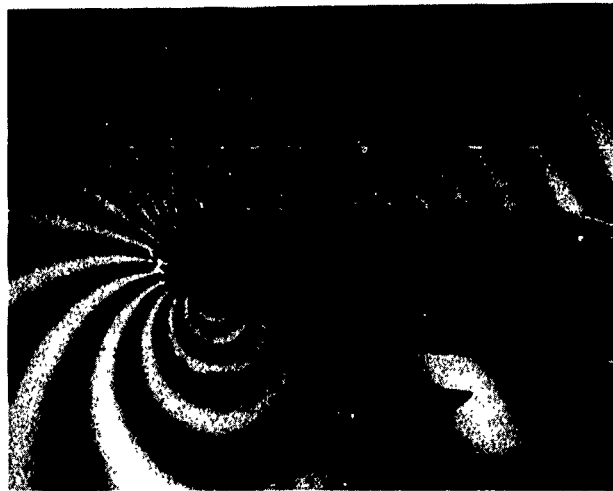Fig. 4. Small Pinhole Interferogram, M = 0.4; (a) $\alpha = 0^0$. (b) $\alpha = 8^0$

Fig. 5 Large Pinhole Interferogram. M = 0.4; (a) $\alpha = 0^0$. (b) $\alpha = 8^0$.

(a)

(a)

(b)

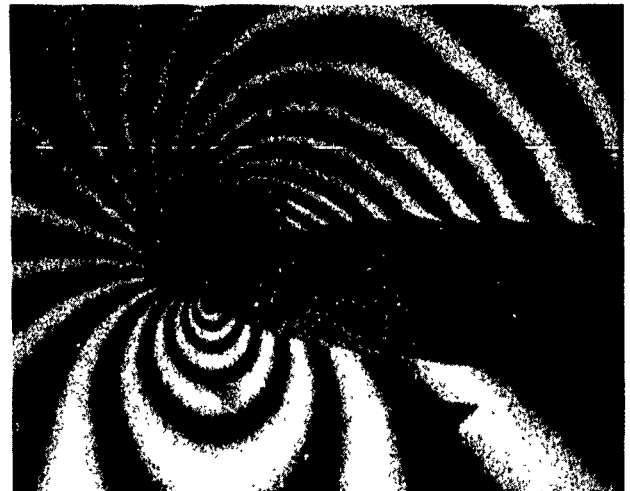(b)

Fig. 6. Large Pinhole Interferogram, Magnified View, M = 0.4; (a) $\alpha = 0^0$, (b) $\alpha = 8^0$.
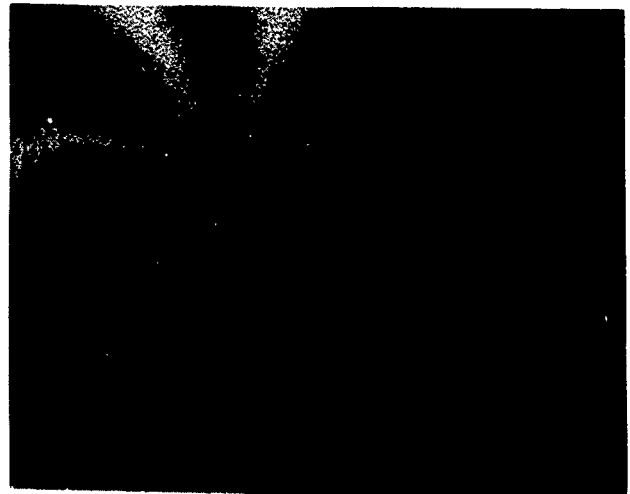
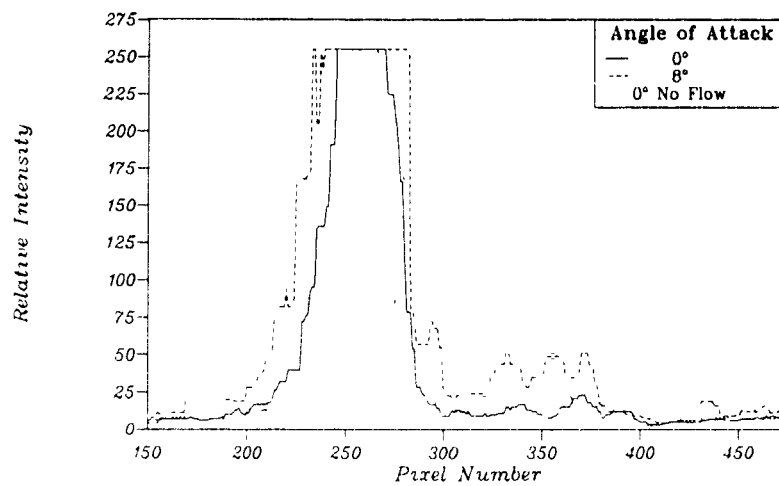Fig. 7. Small Pinhole Interferogram, Photographically Enlarged M = 0.4; (a) $\alpha = 0^0$, (b) $\alpha = 8^0$.

Fig 8 Intensity Distributions at the Focus of Mirror 2.